Strong-field ionization with two-color circularly polarized laser fields

Christopher A. Mancuso, Daniel D. Hickstein, Patrik Grychtol, Ronny Knut, Ofer Kfir, Xiao-Min Tong, Franklin Dollar, Dmitriy Zusin, Maithreyi Gopalakrishnan, Christian Gentry, Emrah Turgut, Jennifer L. Ellis, Ming-Chang Chen, Avner Fleischer, Oren Cohen, Henry C. Kapteyn, and Margaret M. Murnane

Phys. Rev. A **91**, 031402 — Published 25 March 2015

DOI: 10.1103/PhysRevA.91.031402

Strong-field ionization with two-color circularly polarized laser fields

Chris Mancuso[1], Daniel D. Hickstein[1], Patrik Grychtol[1], Ronny Knut[1], Ofer Kfir[2], Xiao-Min Tong[3], Franklin Dollar[1], Dmitriy Zusin[1], Maithreyi Gopalakrishnan[1], Christian Gentry[1], Emrah Turgut[1], Jennifer L. Ellis[1], Ming-Chang Chen[4], Avner Fleischer[2,5], Oren Cohen[2], Henry C. Kapteyn[1], and Margaret M. Murnane[1]

[1] *JILA and Department of Physics, University of Colorado Boulder and NIST, Boulder, CO 80309, USA*

[2] *Solid State Institute and Physics Department, Technion, Haifa, 32000, Israel*

[3] *Division of Material Science, Faculty of Pure and Applied Science, University of Tsukuba, Ibaraki 305-8573, Japan*

[4] *Institute of Photonics Technologies, National Tsing Hua University, Hsinchu 30013, Taiwan and*

[5] *Department of Physics and Optical Engineering, Ort Braude College, Karmiel 21982, Israel*

Strong-field ionization provides fundamental insight into light–matter interactions, encoding the structure of atoms and molecules on the sub-Ångström and sub-femtosecond scales. In this Letter, we explore an important new regime: strong-field ionization by two-color circularly polarized laser fields. In contrast to all past work using linearly polarized drivers, we probe electron trajectories that are driven in a 2D plane, thus separating the tunneling angle from the rescattering angle. This allows us to make several new findings. First, we observe a single-lobed electron distribution for co-rotating fields, and a three-lobed distribution for counter-rotating fields, providing the first experimental validation of the theoretical model explaining the generation of circularly polarized high harmonic light. Second, we discover that there is significant electron-ion rescattering using counter-rotating fields, but not with co-rotating fields. Finally, we show that the rescattered electrons are well separated from the directly-ionized electrons, in striking contrast to similar low-energy structures seen with linearly polarized fields. These findings help overcome the long-standing problem of how to decouple the tunneling and rescattering steps in strong-field ionization, which will enable new dynamic probes of atomic and molecular structure.

PACS numbers: 32.80.Fb, 34.80.Qb, 42.65.Ky

The interaction of intense laser fields (10^{14} Wcm^{-2}) with atoms and molecules is of great scientific and technological interest because of two related phenomena: high-harmonic generation (HHG) [1] and strong-field ionization (SFI) [2, 3]. HHG enables tabletop generation of coherent beams of extreme ultraviolet (EUV) and soft x-ray light [4], which have a broad range of applications. For example, HHG makes it possible to capture chemical reactions in real time [5–7], to uncover correlated charge/spin/phonon dynamics in materials with elemental specificity [8–10], and to perform coherent imaging on the nanometer scale near the wavelength limit [11, 12]. Similarly, recent studies have revealed that the photoelectron distribution from SFI can provide information about dynamic orbital and molecular structure [13–16], indicating its potential for understanding molecular dynamics.

Both HHG and SFI begin with the tunnel-ionization of an electron from an atom or molecule, after which the free electron is accelerated in the laser field [17]. HHG occurs when an electron that is driven back to the parent ion recombines, releasing its kinetic energy by emitting a high-energy photon. SFI results from electrons that do not recombine, but may still re-encounter their parent ion and rescatter. The fact that both recombination (i.e. HHG) and rescattering are strongly suppressed in elliptically or circularly polarized driving laser fields [3, 18–21] means that past studies have generally used linearly polarized light to drive the HHG and SFI processes. However, when using linearly polarized light, field-driven electrons are confined to one-dimensional (1D) trajectories, making it difficult to deconvolve molecular structural information encoded by both the tunnel-ionization and rescattering steps [22–24]. In contrast, using two-color circularly polarized fields, electrons are driven in a two-dimensional (2D) plane [25], allowing the tunneling and rescattering processes to occur at different angles.

In this article, we present the first experimental observation of SFI using two-color circularly polarized laser fields. We make several new observations about SFI under these complex polarization-shaped fields. First, the photoelectron distributions exhibit unusual symmetries: namely a single-lobe crescent shape when the two fields have the same helicity (co-rotating), or a three-lobe shape when the fields have opposite helicity (counter-rotating). Second, low-energy features appear in the photoelectron distribution only when the two laser fields are counter-rotating. Advanced numerical calculations using the time-dependent Schrödinger equation show that these features are due to strong electron-ion rescattering. Finally, we observe that the low-energy rescattered electrons are well separated from those that do not re-encounter the core [3, 26–30]. This demonstration of well-separated electron-ion rescattering structures paves the way for the development of spectroscopies that will steer the 2D electron trajectories (by adjusting intensities, frequencies and ellipticities of the driving fields) in order to provide new probes of atomic and molecular dynamics.

In addition, the observation of the shape and symmetry of the photoelectron distributions resulting from two-color circularly polarized fields provides the first experimental validation of the theoretical model of HHG

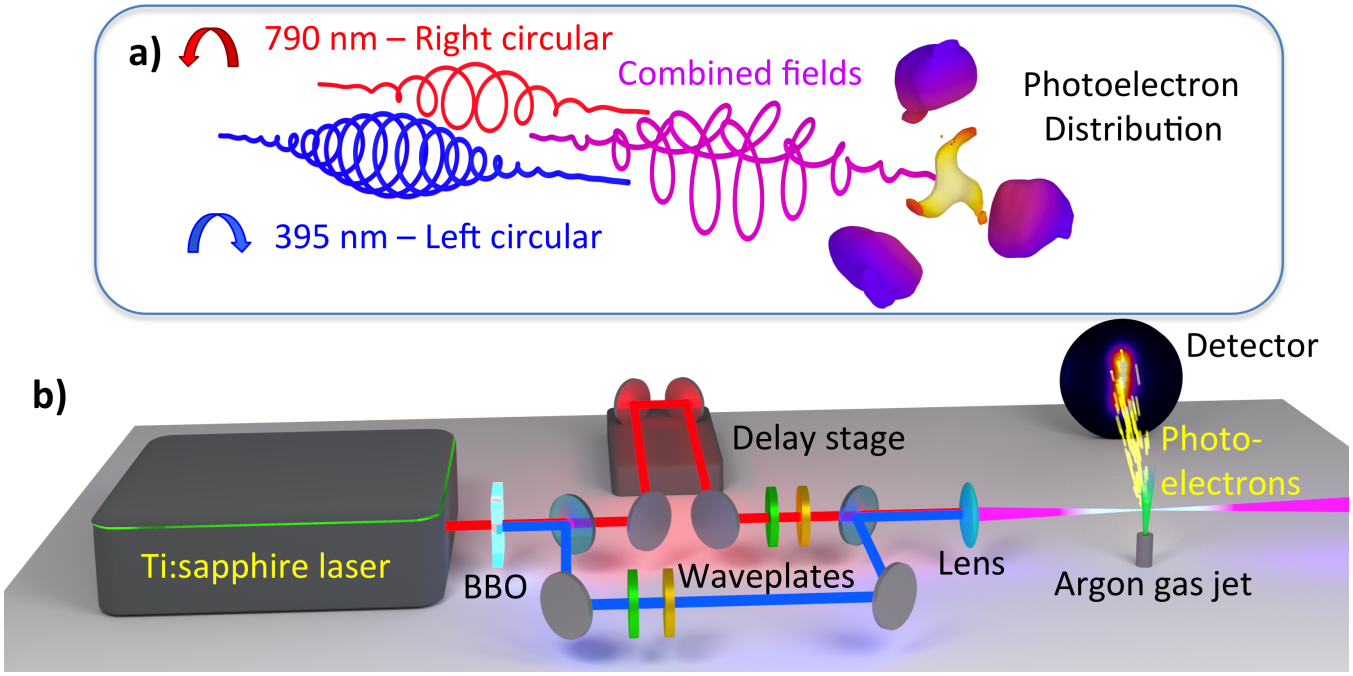

FIG. 1. (color online) (a) Two-color counter-rotating circularly polarized laser fields ionize atoms to produce photoelectron distributions that exhibit distinct features (central yellow lobes) that result from electron-ion rescattering. (b) Experimental apparatus used to detect the photoelectron distributions.

under these fields [25, 31–35]. Recently, HHG driven by counter-rotating fields has been demonstrated as a breakthrough source of coherent circularly polarized EUV light, enabling powerful spectroscopies – such as probing chiral molecules using photoelectron circular dichroism [36, 37] and investigating femtosecond magnetic dynamics using x-ray magnetic circular dichroism [34, 38] – to move from the synchrotron to the tabletop. The theoretical model for HHG under these conditions is built on the idea that electrons can be driven back to the parent ion three times per laser cycle, each time at a different angle. Our observation of three-fold symmetric photoelectron distributions provides the first direct experimental validation of this elegant theoretical model.

To study SFI with two-color circularly polarized fields, we used a velocity map imaging (VMI) spectrometer [39] to record 2D projections of the three-dimensional (3D) photoelectron distributions onto a microchannel-plate–phosphor-screen detector (Beam Imaging Solutions) and a CCD camera [Fig. 1]. The fundamental laser pulses (790 nm, 45 fs) were derived from a Ti:sapphire regenerative laser amplifier (KMLabs Wyvern HP) operating at 4 kHz. The second harmonic (395 nm) was obtained via frequency doubling in a 200 μm thick beta barium borate (BBO) crystal. Dichroic mirrors were used to separate, and later recombine, the fundamental and second harmonic in a Mach–Zehnder geometry [Fig. 1]. A delay stage was placed in the 790 nm arm to control the relative time delay of the laser pulses. Waveplates ($\lambda/4$ and $\lambda/2$) were placed in each beam to separately control the polarization of the 395 nm and 790 nm laser pulses. A one-to-one magnification telescope consisting of two lenses was placed in the 790 nm arm of the delay line to compensate for chromatic aberration in the final focusing lens. The laser pulses were focused into a skimmed supersonic jet of argon gas, with intensities of $\sim 5 \times 10^{13}$ Wcm^{-2} for each of the beams separately. The photoelectron distributions were then recorded as a function of the time delay between the fundamental and the second harmonic, using a step size of $\sim$133 attoseconds. The experiment was carried out by combining the fundamental and second harmonic fields in two distinct cases: with the fields counter-rotating, and with the fields co-rotating.

By recording the photoelectron distributions as a function of time-delay between the 395 nm and 790 nm fields, we make several important discoveries about SFI under two-color circularly polarized fields: 1) The shape of the photoelectron distributions depend on the relative helicities between the circularly polarized fields. 2) The electron distributions rotate with the time-delay between the two laser fields, allowing the 3D photoelectron distribution to be reconstructed using tomographic methods [40–43]. 3) Counter-rotating fields enable electron-ion rescattering (and HHG), which is not present for co-rotating fields.

One noticeable difference in the shape of the photoelectron distribution between the two cases is that the co-rotating circular fields produce higher kinetic energy photoelectrons than the counter-rotating fields. The dif-

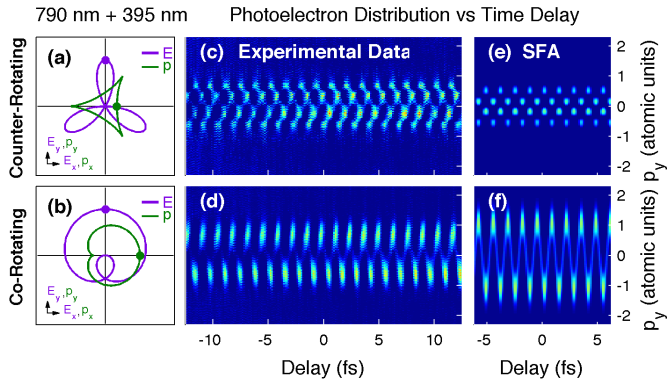

FIG. 2. (color online) (a-b) The combined laser electric field ($\vec{E}$) and final drift momentum of tunnel-ionized electrons ($\vec{p}$), where the dots indicate time zero for $\vec{E}$ and $\vec{p}$. (c-d) Normalized 1D projections of the experimental photoelectron distributions plotted as a function of time delay between the 790 and 395 nm laser pulses, which reveal oscillations due to the rotation of the photoelectron distribution with a period of 1.3 fs (one cycle of the 395 nm field). (e-f) Theoretical photoelectron distributions using the strong-field approximation (SFA) reproduce the qualitative differences between the co-rotating and counter-rotating cases.

ferences in the photoelectron kinetic energies can be explained through a simple analysis of the electric field ($\vec{E}$) that results from the sum of the two laser fields. Within the strong-field approximation (SFA), which ignores the role of the Coulomb potential of the ion, the final drift momentum of the electron is given by $\vec{p}(t_b) = (p_x, p_y) = \int_{t_b}^{\infty} \vec{E}(t)\, dt$, where t_b is the time that the electron tunnels from the atom. To predict the photoelectron distributions, two factors must be considered: $\vec{p}(t_b)$ which is where an electron that tunnels at t_b will impact on the spectrometer, and $\vec{E}$ which determines the probability that an electron will tunnel-ionize at that moment, and therefore the signal intensity on the spectrometer.

In the case of counter-rotating fields, the total electric field vector traces out a trefoil or "three-leaf clover" pattern [Fig. 2(a)], which has three maxima per laser cycle. These three maxima in E correspond to the three minima in final momentum p, which leads to the expectation that the photoelectron distribution from counter-rotating fields should consist of three lobes separated by 120 degrees. In contrast, for the case of co-rotating fields, the electric field has only a single maximum per laser cycle [Fig. 2(b)], and this maximum in E corresponds to a maximum in p. Thus, co-rotating circularly polarized pulses should produce a photoelectron distribution that consists of a single lobe of relatively high kinetic energy electrons. Thus, the most prominent differences in the photoelectron kinetic energies from co- and counter-rotating circularly polarized fields can be explained as a result of electrons that tunnel-ionize near the peak of the two-color laser field and proceed to the detector without re-encountering the parent ion.

To determine the role of electron-ion rescattering in SFI from two-color circularly polarized laser fields, it is necessary to evaluate the complete 3D photoelectron distribution. However, the VMI spectrometer only records a 2D projection on the detector, and the lack of cylindrical symmetry prevents conventional reconstruction techniques [44]. Since the laser propagation direction (z-axis) is parallel to the detector, the plane that contains the 2D electric field created by the two-color circularly polarized field is perpendicular to the detector. This means that the VMI spectrometer can only collect information in one dimension of the laser field (y-axis), whereas information in the other dimension (x-axis) cannot be directly obtained.

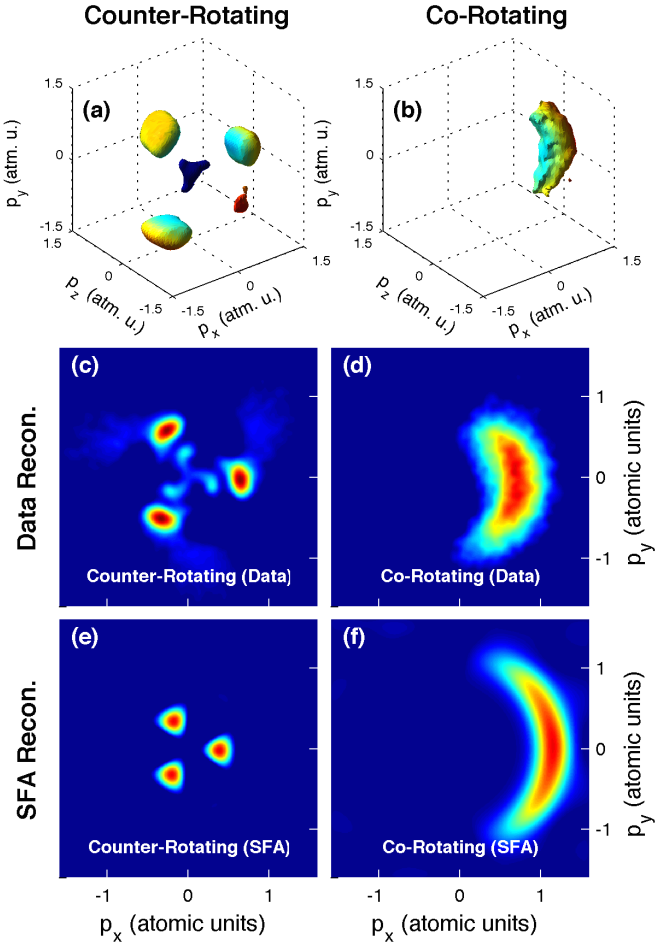

FIG. 3. (color online) (a,b) The experimental 3D photoelectron distribution for both counter- and co-rotating fields. (c-f) 2D projections of the 3D photoelectron distribution are compared to 2D SFA calculations. While the co-rotating data (d) is adequately reproduced by the SFA calculations (f), the counter-rotating case (c) exhibits low-energy structures that do not appear in the SFA model (e).

Fortunately, one of the unique aspects of circularly po-

larized laser fields produced by combining the fundamental and second harmonic fields is that the electric field distribution can be rotated in the laboratory frame simply by changing the time-delay between the two laser pulses [45]. Normalized sinograms were created through three data processing steps. First, each time-delay step was averaged over the laser propagation direction. Second, we divide the photoelectron distribution for each time step by its mean value in order to remove the fact that the total photoelectron yield changes for each time-delay step, which is simply due to the cross-correlation of the laser pulses. Finally, the non-rotating component of the distributions consisting of electrons generated in regions where the pulses do not overlap was subtracted out to better highlight the oscillatory features of the distributions.

These normalized sinograms show that for counter-rotating fields [Fig. 2(c)], the three-lobed distribution rotates 120 degrees in one cycle of the second harmonic (1.3 fs). For co-rotating fields [Fig. 2(d)], the single-lobed distribution makes one full revolution for every cycle of the second harmonic. In both cases, the photoelectron distribution returns to a point of symmetry every 1.3 fs, as is seen in the experimental data [Figs. 2(c,d)]. These oscillating distributions can be modeled by weighting the final drift momentum by the tunnel-ionization rate [29] over a number of different relative time delays of the two laser pulses [Fig. 2(e,f)]. This ability to arbitrarily rotate the photoelectron distribution allows for the reconstruction of the 3D photoelectron distribution using tomographic reconstruction techniques [40–43]. By applying the inverse Radon transform [46] to each slice in the laser propagation (z) direction, a complete 3D reconstruction of the photoelectron distribution is obtained [Fig. 3(a,b)]. The photoelectron distribution resulting from the counter-rotating case manifests as a three-lobed shape with significant electron density near zero kinetic energy.

By examining 2D projections of the 3D photoelectron distributions, we can easily observe additional features that are indicative of the continuum dynamics of laser driven electrons. We compare the experimental photoelectron distributions [Fig. 3(c,d)] with the distributions predicted using the SFA [Fig. 3(e,f)], which ignores any effect of the Coulomb potential of the parent ion. The SFA adequately reproduces the co-rotating case. However for the counter-rotating case, the SFA model matches the symmetry and the kinetic energy of the experimental photoelectron distributions, but there is a significant difference: the experimental photoelectron distribution has a low-energy structure that is not captured by the simple model. The absence of this structure from the model suggests that it is a result of the interaction between the Coulomb potential of the parent ion and the returning electrons.

To further understand how the low-energy structures depend on the Coulomb potential, the 3D time-dependent Schrödinger equation (TDSE) is solved us-

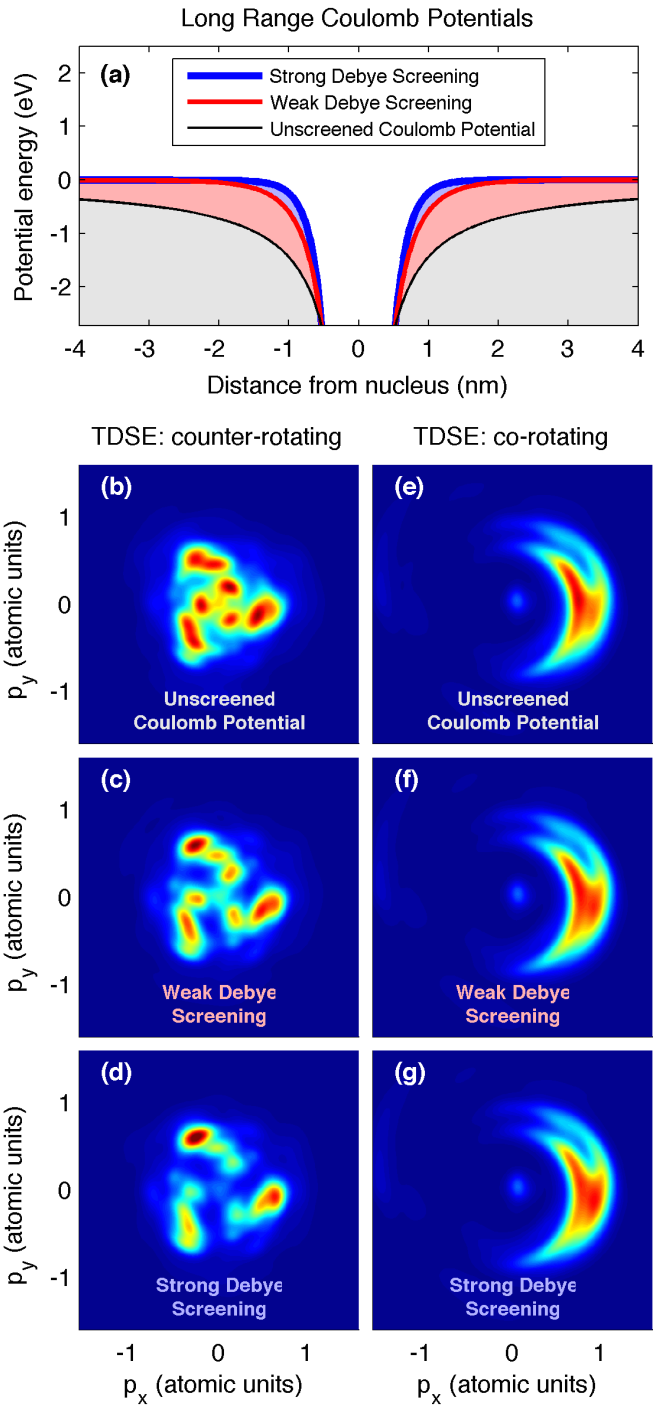

FIG. 4. (color online) Time-dependent Schrödinger equation (TDSE) simulations investigating the effects of the Coulomb potential. (a) The electron-nuclear potentials used in the TDSE calculations. (b-d) For the counter-rotating case, the low-energy structures disappear as the screening factor for the Coulomb potential is increased, confirming that the low-energy structures are due to strong electron-ion rescattering. (e-g) In the co-rotating case no change as as the screening factor is varied, indicating the absence of rescattering.

ing a generalized pseudospectral method [47, 48]. To isolate the effect of the Coulomb potential, we "turned off" the influence of the long-range Coulomb potential by adding a Debye screening factor starting at an electron-ion distance of $r = 10$ atomic units of the form $exp[-(r-10)/r_a]$. The screening factor r_a was set at ∞, 10 and 5 atomic units, which corresponds to a unscreened Coulomb potential, a weakly screened Coulomb potential, and a strongly screened Coulomb potential, respectively [Fig. 4(a)]. The simulations assume an intensity of 5×10^{13} Wcm^{-2} for each color.

The simulated photoelectron distributions are in very good agreement with the experimental data, reproducing the energies, symmetries, and general shape of the photoelectron distributions for both the co- and counter-rotating fields. In the case of the co-rotating fields [Fig. 4(e-g)], there is little effect observed from varying the screening of the Coulomb potential, indicating that the tunnel-ionized electrons are not driven back near the parent ion. However, for the counter-rotating field [Fig. 4(b-d)], the inner structures are strongly influenced by the presence of the Coulomb potential, confirming that the laser field drives the electrons in close proximity to the ion.

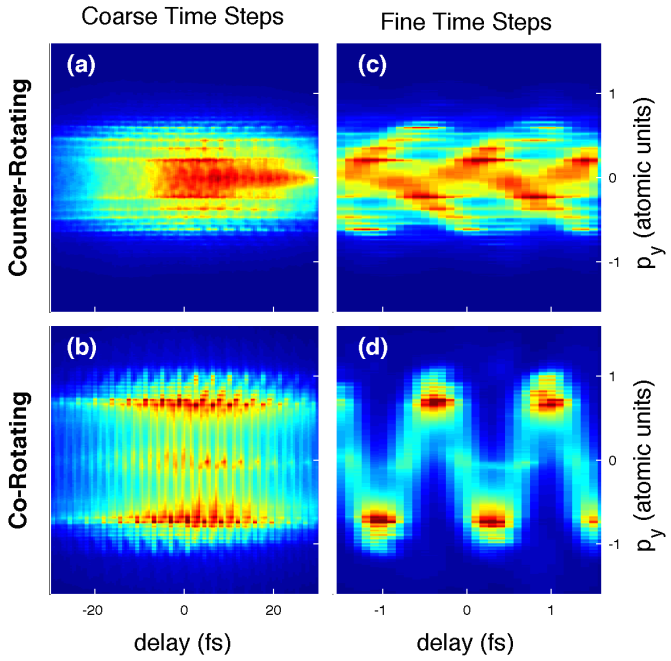

FIG. 5. (color online) (a,b) Coarse time step TDSE simulations reveal the change in the photoelectron yield due to the cross-correlations between the two laser pulses, and oscillations every 1.33 fs. In the co-rotating case, most of the electrons are driven to higher-kinetic energies, whereas a large number of low-energy electrons can be seen in the counter-rotating case. (c,d) Fine time step TDSE simulations show good agreement with the experimentally observed sinograms presented in Fig. 2(c,d).

In summary, we made the first observations of the 3D photoelectron distributions resulting from the strong-field ionization by two-color circularly polarized laser fields, providing the first experimental validation for the theory of high-harmonic generation in this important new regime. We found that the general shape and symmetry of the photoelectron distributions is well explained by a simple strong-field model, which ignores the Coulomb potential of the ion. However, in the case of counter-rotating two-color fields, we observed low-energy structures in the photoelectron distribution, indicating the presence of electron-ion rescattering. Numerical simulations using the time-dependent Schrödinger equation confirm that the Coulomb potential is responsible for the appearance of the low-energy electrons. Importantly, both the experiment and theory indicate that the rescattered electrons are well-separated in energy from those electrons that do not re-encounter the ion, indicating that strong-field ionization using these complex polarization-shaped fields may lead to breakthrough techniques for studying atomic and molecular dynamics.

ACKNOWLEDGMENTS

The experimental work was done at JILA, with funding from the U.S. Department of Energy Office of Basic Energy Sciences AMOS program and from the Physics Frontiers Center Program. JILA also gratefully acknowledges support from an AFOSR DURIP award for the laser system used for this work. CM acknowledges support from the National Science Foundation Graduate Research Fellowship under Grant No. DGE 1144083. PG acknowledges support from the Deutsche Forschungsgemeinschaft #GR 4234/1–1. RK acknowledges the Swedish Research Council (VR) for their financial support. This work was supported by the USA-Israel Binational Science Foundation (BSF). The Technion group is part of the Israeli Center of Research Excellence Circle of Light supported by the I-CORE Program of the Planning and Budgeting Committee and The Israel Science Foundation. XMT was supported by a Grant-in-Aid for Scientific Research (Grant No. C24540421) from the JSPS and the HA-PACS Project for advanced interdisciplinary computational sciences by exa-scale computing technology. XMT thanks Prof. K. Yabana for helpful discussions.

Appendix: Time-delay TDSE simulations

In order to confirm the experimentally observed time-dependent photoelectron distributions [Fig. 2(c,d)], we undertook TDSE simulations [47, 48] using various time-delays of the laser pulses. The photoelectron distributions from the TDSE simulations were obtained using two different conditions: 1) A long (60 fs) scan, using 0.5 fs steps [Fig. 5(a,b)] and 2) A short (3.2 fs) scan, using 0.1

fs steps [Fig. 5(c,d)]. The long scan reveals the change in the photoelectron yield due to the cross-correlations between the two laser pulses, and both cases reveal oscillations every 1.33 fs. In the co-rotating case, a majority of the photoelectrons in the co-rotating case are driven to higher-kinetic energies, whereas the counter-rotating fields produce significantly lower energy electrons. This agrees well with the experimental data shown in Fig. 2(c,d).

[1] A. Mcpherson, G. Gibson, H. Jara, U. Johann, T. S. Luk, I. A. Mcintyre, K. Boyer, and C. K. Rhodes, J. Opt. Soc. Am. B **4**, 595 (1987).

[2] P. Agostini, F. Fabre, G. Mainfray, G. Petite, and N. Rahman, Phys. Rev. Lett. **42**, 1127 (1979).

[3] D. D. Hickstein, P. Ranitovic, S. Witte, X.-M. Tong, Y. Huismans, P. Arpin, X. Zhou, K. E. Keister, C. Hogle, B. Zhang, C. Ding, P. Johnsson, N. Toshima, M. J. J. Vrakking, M. M. Murnane, and H. C. Kapteyn, Phys. Rev. Lett. **109**, 073004 (2012).

[4] T. Popmintchev, M.-C. Chen, P. Arpin, M. M. Murnane, and H. C. Kapteyn, Nature Photon. **4**, 822 (2010).

[5] X. Zhou, P. Ranitovic, C. W. Hogle, J. H. D. Eland, H. C. Kapteyn, and M. M. Murnane, Nature Phys. **8**, 232 (2012).

[6] E. Gagnon, P. Ranitovic, X.-M. Tong, C. L. Cocke, M. M. Murnane, H. C. Kapteyn, and A. S. Sandhu, Science **317**, 1374 (2007).

[7] W. Li, X. Zhou, R. Lock, and S. Patchkovskii, Science **322**, 1207 (2008).

[8] C. La-O-Vorakiat, M. Siemens, M. M. Murnane, H. C. Kapteyn, P. Grychtol, R. Adam, C. M. Schneider, J. M. Shaw, H. Nembach, and T. J. Silva, Phys. Rev. Lett. **103**, 257402 (2009).

[9] C. La-O-Vorakiat, E. Turgut, C. A. Teale, H. C. Kapteyn, M. M. Murnane, S. Mathias, M. Aeschlimann, C. M. Schneider, J. M. Shaw, H. T. Nembach, and T. J. Silva, Phys. Rev. X **2**, 011005 (2012).

[10] K. Hoogeboom-Pot, D. Nardi, J. N. Hernandez-Charpak, E. Anderson, X. Gu, R. Yang, H. Kapteyn, and M. Murnane, ArXiv preprint , 1407.0658 (2014).

[11] M. D. Seaberg, D. E. Adams, E. L. Townsend, D. A. Raymondson, W. F. Schlotter, Y. Liu, C. S. Menoni, L. Rong, C.-C. Chen, J. Miao, H. C. Kapteyn, and M. M. Murnane, Opt. Express **19**, 22470 (2011).

[12] R. Sandberg, A. Paul, D. Raymondson, S. Hädrich, D. Gaudiosi, J. Holtsnider, R. Tobey, O. Cohen, M. Murnane, H. Kapteyn, C. Song, J. Miao, Y. Liu, and F. Salmassi, Phys. Rev. Lett. **99**, 098103 (2007).

[13] C. I. Blaga, J. Xu, A. D. DiChiara, E. Sistrunk, K. Zhang, P. Agostini, T. A. Miller, L. F. DiMauro, and C. D. Lin, Nature **483**, 194 (2012).

[14] J. Xu, Z. Chen, A.-T. Le, and C. D. Lin, Phys. Rev. A **82**, 033403 (2010).

[15] J. Xu, C. I. Blaga, K. Zhang, Y. H. Lai, C. D. Lin, T. A. Miller, P. Agostini, and L. F. DiMauro, Nat. Commun. **5**, 4635 (2014).

[16] W. Li, A. A. Jaro-Becker, C. W. Hogle, V. Sharma, X. Zhou, A. Becker, H. C. Kapteyn, and M. M. Murnane, Proc. Natl. Acad. Sci. U.S.A. **107**, 20219 (2010).

[17] P. B. Corkum, Phys. Rev. Lett. **71**, 1994 (1993).

[18] P. Dietrich, N. Burnett, M. Ivanov, and P. Corkum, Phys. Rev. A **50**, R3585 (1994).

[19] F. Weihe, S. Dutta, G. Korn, D. Du, P. Bucksbaum, and P. Shkolnikov, Phys. Rev. A **51**, R3433 (1995).

[20] Y. Huismans, A. Rouzée, A. Gijsbertsen, J. H. Jungmann, A. S. Smolkowska, P. S. W. M. Logman, F. Lépine, C. Cauchy, S. Zamith, T. Marchenko, J. M. Bakker, G. Berden, B. Redlich, A. F. G. van der Meer, H. G. Muller, W. Vermin, K. J. Schafer, M. Spanner, M. Y. Ivanov, O. Smirnova, D. Bauer, S. V. Popruzhenko, and M. J. J. Vrakking, Science **331**, 61 (2011).

[21] C. T. L. Smeenk, L. Arissian, B. Zhou, A. Mysyrowicz, D. M. Villeneuve, A. Staudte, and P. B. Corkum, Phys. Rev. Lett. **106**, 193002 (2011).

[22] J. Küpper, Nature Phys. **10**, 550 (2014).

[23] M. Meckel, A. Staudte, S. Patchkovskii, D. M. Villeneuve, P. B. Corkum, R. Dörner, and M. Spanner, Nature Phys. **10**, 594 (2014).

[24] D. Shafir, Y. Mairesse, D. M. Villeneuve, P. B. Corkum, and N. Dudovich, Nature Phys. **5**, 412 (2009).

[25] A. Fleischer, O. Kfir, T. Diskin, P. Sidorenko, and O. Cohen, Nature Photon. **8**, 543 (2014).

[26] C. I. Blaga, F. Catoire, P. Colosimo, G. G. Paulus, H. G. Muller, P. Agostini, and L. F. DiMauro, Nature Phys. **5**, 335 (2009).

[27] F. H. M. Faisal, Nature Phys. **5**, 319 (2009).

[28] C. Liu and K. Z. Hatsagortsyan, Phys. Rev. Lett. **105**, 113003 (2010).

[29] T.-M. Yan, S. Popruzhenko, M. J. J. Vrakking, and D. Bauer, Phys. Rev. Lett. **105**, 253002 (2010).

[30] C. Lemell, K. Dimitriou, X.-M. Tong, S. Nagele, D. Kartashov, J. Burgdörfer, and S. Gräfe, Phys. Rev. A **85**, 011403(R) (2012).

[31] W. Becker, R. Kopold, and D. B. Milos, Phys. Rev. A **61**, 063403 (2000).

[32] W. Becker and D. B. Milos, Phys. Rev. A **62**, 011403(R) (2000).

[33] H. Eichmann, A. Egbert, and S. Nolte, Phys. Rev. A **51**, 3414 (1995).

[34] O. Kfir, P. Grychtol, E. Turgut, R. Knut, D. Zusin, D. Popmintchev, T. Popmintchev, H. Nembach, J. M. Shaw, A. Fleischer, H. Kapteyn, M. Murnane, and O. Cohen, Nature Photon. , Online DOI: 10.1038/NPHOTON.2014.293 (2014).

[35] E. Pisanty, S. Sukiasyan, and M. Ivanov, Phys. Rev. A **90**, 043829 (2014).

[36] N. Böwering, T. Lischke, B. Schmidtke, N. Müller, T. Khalil, and U. Heinzmann, Phys. Rev. Lett. **86**, 1187 (2001).

[37] A. Ferré, C. Handschin, M. Dumergue, F. Burgy, A. Comby, D. Descamps, B. Fabre, G. A. Garcia, R. Géneaux, L. Merceron, E. Mével, L. Nahon, S. Petit, B. Pons, D. Staedter, S. Weber, T. Ruchon, V. Blanchet, and Y. Mairesse, Nature Photon. , Online DOI: 10.1038/NPHOTON.2014.314 (2014).

[38] G. Schütz, M. Knülle, and H. Ebert, Phys. Scripta **T49A**, 302 (1993).
[39] A. T. J. B. Eppink and D. H. Parker, Rev. Sci. Instrum. **68**, 3477 (1997).
[40] M. Wollenhaupt, C. Lux, M. Krug, and T. Baumert, ChemPhysChem **14**, 1341 (2013).
[41] C. Smeenk, L. Arissian, A. Staudte, D. M. Villeneuve, and P. B. Corkum, J. Phys. B **42**, 185402 (2009).
[42] D. Dimitrovski, J. Maurer, H. Stapelfeldt, and L. B. Madsen, Phys. Rev. Lett. **113**, 103005 (2014).
[43] J. Ambrose and G. Hounsfield, Br. J. Radiol. **46**, 148 (1973).
[44] V. Dribinski, A. Ossadtchi, V. A. Mandelshtam, and H. Reisler, Rev. Sci. Instrum. **73**, 2634 (2002).
[45] "See Supplamental Material for videos that show the rotation of: 1) the electric field and final drift momentum and 2) the photoelectron distributions capture in the velocity map imaging spectrometer.".
[46] A. C. Kak and M. Slaney, *Principles of Computerized Tomographic Imaging* (IEEE Press, 1988).
[47] X. Tong, K. Hino, and N. Toshima, Phys. Rev. A **74**, 031405 (2006).
[48] X.-M. Tong and S.-I. Chu, Phys. Rev. A **58**, R2656 (1998).